

Article

Development and Analysis of a Modular LED Array Light Source

Stefan Mitterhofer ^{1,*} , Žiga Korošak ^{1,2}, Žiga Rojec ¹, Marko Jankovec ¹  and Marko Topič ¹ 

¹ Faculty of Electrical Engineering, University of Ljubljana, Tržaška Cesta 25, 1000 Ljubljana, Slovenia; ziga.korosak@st.com (Ž.K.); Ziga.Rojec@fe.uni-lj.si (Ž.R.); Marko.Jankovec@fe.uni-lj.si (M.J.); Marko.Topic@fe.uni-lj.si (M.T.)

² STMicroelectronics d.o.o, Tehnološki Park 21, 1000 Ljubljana, Slovenia

* Correspondence: stefan.mitterhofer@fe.uni-lj.si

Received: 9 September 2020; Accepted: 12 October 2020; Published: 14 October 2020



Abstract: Light emitting diodes (LEDs) have experienced rapid technological development in the past decade, making them a winning alternative to conventional light sources in many applications. LED arrays allow precise control of the desired irradiance profile in a target area by adjusting the position and output power of individual LEDs. However, despite increased efficiency, many LEDs still transform a large proportion of the input electrical power into heat, requiring an efficient cooling system. This paper presents a modular LED array light source mounted on a water-cooled aluminum plate. Novel electronic LED driver modules, connected via a serial communication bus in a daisy-chain topology, were developed with the ability to set the operating current of individual LEDs. A modular layout of cooling and mounting system and LED driver modules, as well as a specialized design for the LED soldering footprint, was able to house a variety of common commercial LEDs, enabling easy adjustment of the lighting system to the required application and size of the irradiated area. In a prototype of one plate containing 10 LEDs, individual LED radiance was optimized for a better irradiance homogeneity in the target area. Array characterization showed a low standard deviation of the irradiance of 1.8% and a good fit between measured and calculated irradiance. A test of the array at elevated temperatures showed moderate LED radiance degradation and a wavelength shift of the measured spectra after extended use.

Keywords: light emitting diode; lighting system; irradiance optimization; degradation

1. Introduction

More than 15% of the global electricity demand is stemming from lighting applications [1]. Recent efforts to reduce its ecological footprint along with the prospering market resulted in a remarkable progress of light emitting diode (LED) technology, especially in the past two decades. LEDs have become a winning alternative to traditional light sources for various applications [1,2]. Their advantages include a long lifetime, high efficiency, and, consequently, lower heat dissipation [3]. LEDs available on the market cover a wide spectrum of emitted light, encompassing ultraviolet (UV) and visible and infrared (IR) light [4,5]. Their possible applications are correspondingly numerous. LEDs emitting visible light are used, for example, in phone and tablet displays, television monitors, and domestic lighting [1]. LEDs of various colors are illuminating displays and the internal space of cars [6]. They are further used for hydroponic plant growth [7]. The solar spectrum can be approximated with systems of various types of LEDs for photovoltaic (PV) module characterization [8]. UV LEDs are used, for example, to cleanse water by degrading organic pollutants in water, for example, dyes, pharmaceuticals, and insecticides [9,10]. Other applications include fluorescence detection [11], curing [12], photolithography [13], and biomedical research [14].

The small LED footprint enables their placement in dense arrays, achieving possible high-power densities and control over the irradiance distribution in the target area. A homogeneous irradiance can be achieved in a small target area by corresponding LED placement [15,16] or diffusive elements [17,18]. Various types of LEDs can be combined to achieve the desired spectral irradiance profile [16–18]. Larger irradiated areas require adjustment of individual LED position and radiance [14,19–21]. While small arrays containing a low number of LEDs can easily be adjusted manually [14] or with common general optimization algorithms [21], these methods can be unsuitable for the optimization of large arrays containing a high number of LEDs and a correspondingly high number of optimization parameters due to either inaccurate results or exorbitant computation times.

Commonly, LED arrays are designed with a specific purpose in mind, which sets limited requirements of the required irradiated area [8,11,12,14,16–19]. However, some research fields require a modular and easily adjustable array design. For example, analyzed samples in PV can range from individual polymeric material samples [22], laminates [23], or research cells [24] over mini-modules [25] to full-sized commercial modules [26]. The required irradiated areas range from a few square millimeters to several square meters.

Such arrays dissipate a lot of electric energy into heat, especially when low-efficiency LEDs are densely packed [19,27]. Consequently, high LED temperature is decreasing their output radiance, causing faster degradation and possibly a wavelength shift of the emitted light [27]. Some applications can require such arrays to be used in extreme conditions, such as elevated temperature [14] or humidity. Thus, efficient cooling of the array is required.

This paper presents the design, manufacture, and analysis of a modular water-cooled LED array. Section 2 presents the design. It shows, first, a method for calculating and optimizing the irradiance homogeneity by adjusting LED placement and individual radiance. We further present the designs of novel electronic drivers and a corresponding control unit, able to operate a variable number of LEDs, and of a modular mounting and cooling system for the array. Section 3 presents the manufacture of a prototype array with UV LEDs. Two experiments are described for the array characterization. First, we measured the spatial irradiance profile in the target area to verify the irradiance calculations. Second, we tested the light source’s stability at severely elevated temperature and humidity conditions inside a climatic chamber and evaluated degradation of LEDs and drivers in such conditions. Section 4 presents the results of these experiments as well as of the array optimization.

2. Array Design

2.1. Irradiance Homogeneity Optimization

An array of homogeneously spread LEDs operating at their nominal current causes a stronger irradiance in front of the center of the array compared to its edges, especially for wide-angle LEDs [28]. Thus, two parameters were optimized for the design of the array: The distance between the LEDs and the radiance of individual LEDs. We developed an iterative method for irradiance homogeneity optimization of an LED array in a flat target area [28,29]. The angular radiance distribution was approximated as a non-perfect Lambertian emitter [30].

$$E(r, \theta) = E(r, 0) \cdot \cos^m \theta \tag{1}$$

$E(r, \theta)$ is the irradiance at distance r under the viewing angle θ . The parameter m describes the radiance distribution of the non-perfect Lambertian emitter. It is correlated to the viewing angle $\theta_{1/2}$, at which the irradiance is at half the maximum.

$$m = -\frac{\ln 2}{\ln(\cos \theta_{1/2})} \tag{2}$$

The irradiance $E(x, y)$ at point (x, y) is calculated by summing up the contributions of all LEDs, which are placed homogeneously in an $N \times M$ array. N and M are positive integers and define the

number of LEDs in the array. Considering furthermore the inverse-square law and a reduction of the irradiance with the cosine of the angle of incidence, $E(x,y)$ is given by:

$$\begin{aligned}
 E(x,y) &= \sum_{i=1}^N \sum_{j=1}^M I_{ij} \cdot \cos^m \theta_{ij} \cdot \cos \theta_{ij} \cdot \frac{1}{r_{ij}^2} \\
 &= z^{m+1} \sum_{i=1}^N \sum_{j=1}^M I_{ij} \cdot r_{ij}^{-m-3}.
 \end{aligned}
 \tag{3}$$

The angle θ_{ij} is the viewing angle at point (x, y) for the LED number (i, j) . I_{ij} is the irradiance on a target at a distance of $z = 1$ m at an angle $\theta_{ij} = 0^\circ$ of only LED number (i, j) . The distance r_{ij} between the point (x, y) on the target plane and the LED (i, j) is:

$$r_{ij} = \sqrt{[x - x_0]^2 + [y - y_0]^2 + z^2} = \sqrt{[x - d \cdot (i - 1)]^2 + [y - d \cdot (j - 1)]^2 + z^2}.
 \tag{4}$$

The distance between the LEDs in x and y directions is d . The irradiance at any point of the target surface can be calculated using the Equations (3) and (4). We then split the target area into $N \times M$ evenly sized rectangles, each corresponding to one LED.

In the first step, all LEDs were set to 100% relative power. The average irradiances in the rectangles $E_{i,j}$ and the average irradiance over the entire plate E_P were calculated. For the next iteration step, the relative power of the LEDs was adjusted to change $E_{i,j}$ to a target irradiance E_{target} . It was defined by:

$$E_{target} = \frac{E_P + \frac{M+N}{4} \cdot E_{i,j}}{1 + \frac{M+N}{4}}.
 \tag{5}$$

This arbitrary function converged toward E_P as the irradiances in the individual rectangles converged. It was defined for a better stability of the algorithm. While all LEDs were changed during this step, in general, the changes of other LEDs during the same iteration step were not considered. E_P and $E_{i,j}$ were recalculated only after all LEDs were adjusted individually. We used the symmetry of the array geometry to reduce the number of parameters, similar to the first optimization method. So, not every LED had to be calculated.

These two steps (radiance adjustment and irradiance recalculation) were repeated until a homogeneous irradiance in the target area was found. The distance between LEDs d was then adjusted and the process repeated in search of a better homogeneity. Figure 1 shows a flowchart of this process. The distance z between array and target can be adjusted and the optimization repeated, if a higher irradiance is required.

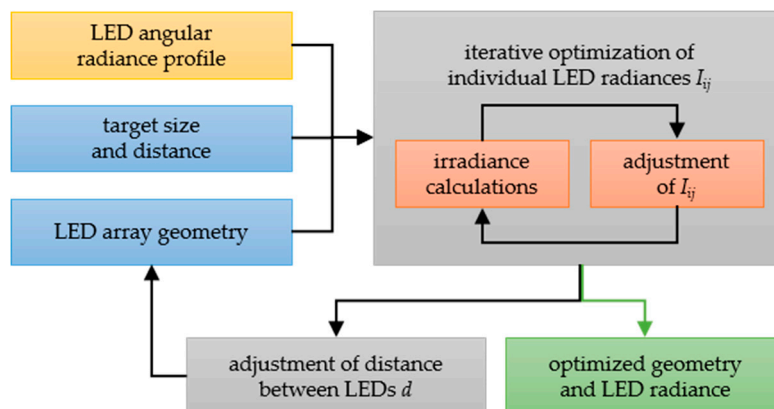


Figure 1. Flowchart showing the main steps of the optimization process. The output (green) is given when either a maximal number of iterations is reached or no better homogeneity is found.

This iterative method is very fast and can optimize large arrays containing hundreds of LEDs in a matter of seconds. However, it cannot optimize small LED arrays with inhomogeneous LED placement. This shortcoming is related to certain blind spots on the target area in such cases. Other methods are better suited for such tasks, for example, using common optimization algorithms like Genetic Algorithm (GA) and Pattern Search (PS) [21].

2.2. Electronic LED Drivers

A modular system was constructed to allow for a flexible lighting solution [31]. The system was composed of LED lighting modules and a module control unit. The block diagram is shown in Figure 2a. A variable number of lighting modules was supported, up to 200 in total. The communication between modules and the control unit used a universal asynchronous receiver-transmitter (UART) interface in daisy-chain topology. The control unit addressed the modules in the chain by their position. The current on each module was set individually. The modules measured current of the LEDs to allow for regulation of output radiance. The block diagram of the individual lighting modules is shown in Figure 2b. Each module had its own power supply, enabling the construction of an array with different types of LEDs and required supply voltage.

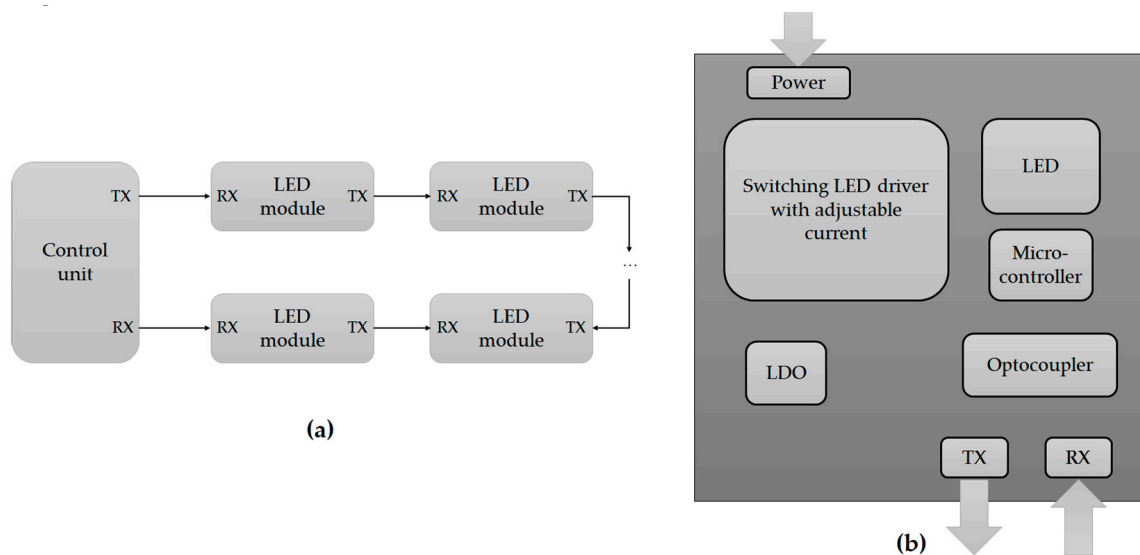


Figure 2. (a) Lighting system block diagram. (b) LED lighting module block diagram. TX: Transmitter, RX: Receiver, LDO: Voltage regulator.

The power supply voltage range was 4.5–42 V. The minimum voltage depended on the voltage drop of the used LED at maximal current. As switching controller of the LED driver, a TPS92513 constant-current buck controller (Texas Instruments, Dallas, TX, USA) was used. The controller can deliver output current of up to 1.5 amperes with up to 97 % conversion efficiency. In this design, the output current was limited to 850 mA. It allowed both analog and pulse-width modulation (PWM) to control the output of the LED. An ATtiny816 microcontroller (Microchip Technology Inc, Chandler, AZ, USA) was chosen to adjust the output current of the LED. It enabled UART communication and measurement of current and temperature at an extremely small package size and power consumption. A TLS805B1 linear voltage regulator (Infineon Technologies AG, Neubiberg, Germany) was used to provide 1.8 V of power supply voltage to the microcontroller. Additionally, an optocoupler on the communication line accounted for possible shifts in ground potential between the lighting modules and prevented failure progress in the system. The LED modules were connected in a daisy-chain topology, where each module passed the message to the next adjacent module until the whole array was updated with the new settings. Thus, only two communication lines were required for the whole LED array for a full-duplex serial communication.

The modules were constructed on a single-layer aluminum printed circuit board (PCB) to maximize cooling and measured just 30 mm × 30 mm to enable dense driver and LED placement. The LED footprint on the lighting modules was specially designed to allow for soldering of various common types of LEDs from different manufacturers, for example LZ4-00CW08 white LEDs (LED Engin Inc., San Jose, CA, USA), GH CSSRM4.24 red LEDs (OSRAM Opto Semiconductors, Munich, Germany), the C03 UV product series (Lite-On, Taipei, Taiwan), or the XLamp XP-E LED series (Cree Inc., Research Triangle Park, NC, USA) covering a multitude of colors. A circuit diagram of the module is shown in Figure 3. The layout and an image of an assembled one are shown in Figure 4.

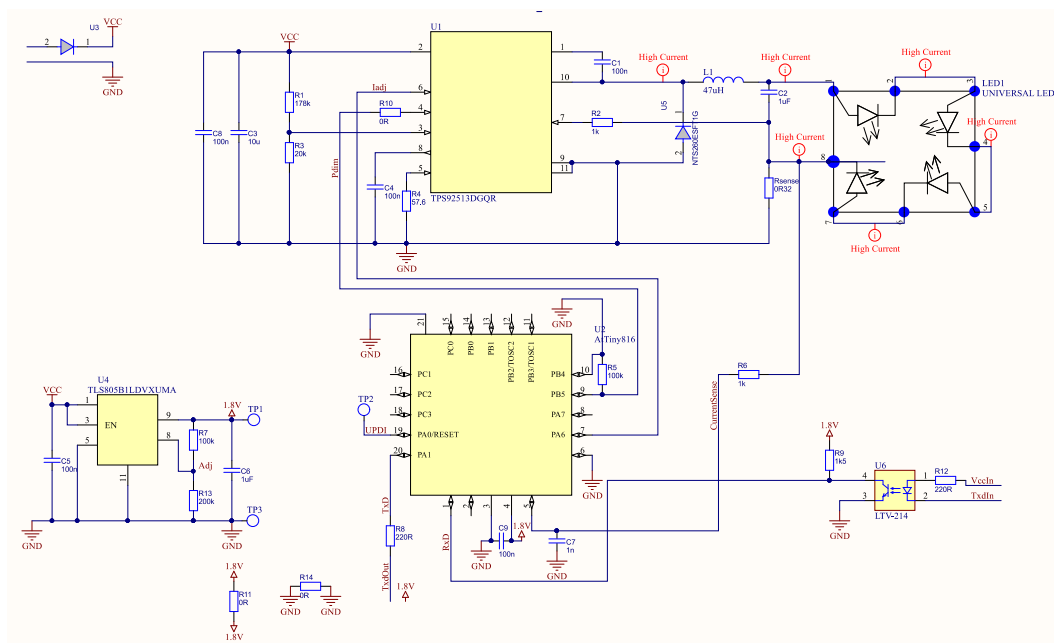


Figure 3. Schematic of the drivers’ circuit.

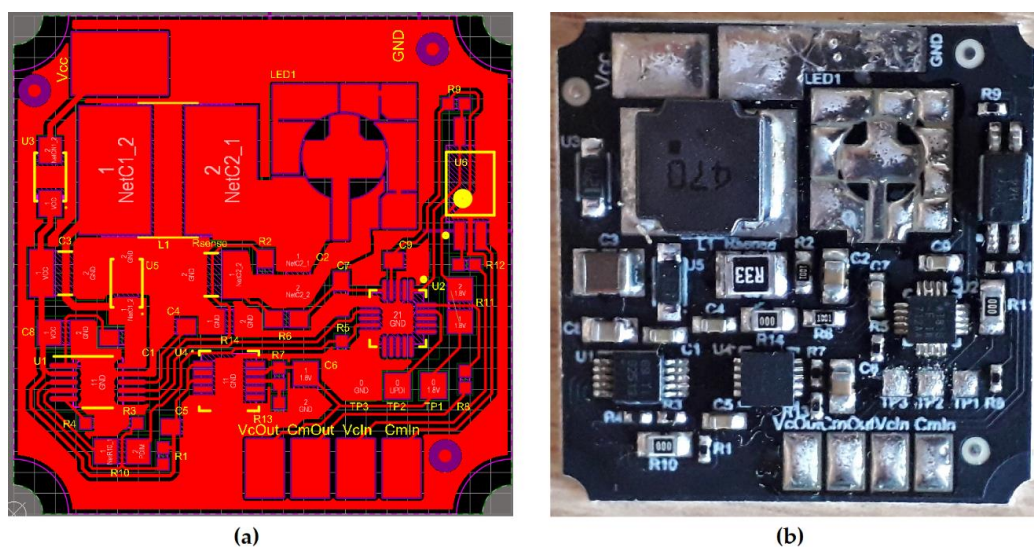


Figure 4. (a) Layout of the LED lighting module. (b) Image of an assembled driver (without LED).

The output current of the LED driver was measured at different current settings with several modules and two different types of LEDs, VLMU3500-385-060 (Vishay Intertechnology Inc., Malvern, PA, USA) and LZ4-04UV00. The maximum current in these measurements was

limited to the nominal current for the LEDs, up to 500 mA (VLMU3500-385-060) and 700 mA (LZ4-04UV00), respectively.

The module controller was designed for easy programming of LED modules through a graphical user interface or with a PC through a console. It was based around SAM3S4B microcontroller (Microchip Technology Inc., Chandler, AZ, USA) and can be powered via USB or from the same power supply as LED modules. It can save several module configurations in its flash memory and, thus, does not have to be configured every time it is powered on. Configurations can have different numbers of connected modules each, and, upon power on an appropriate configuration, will be chosen according to the number of currently connected modules.

2.3. Mounting and Cooling of the Array

LEDs are generally less efficient, degrade faster, and experience a wavelength shift when operating at higher temperatures. Thus, an aluminum (Al) plate was designed as a base for the array. Channels on the backside were grooved for water cooling. A Plexiglas plate resistant to high temperatures was screwed onto it. This plate pressed down a rubber gasket inside a groove in the Al to seal the channels to avoid water leakage. A double-sided sealing tape between the two plates served as additional protection. Water inlet and outlet were screwed onto the Plexiglas plate. The LED drivers were mounted on the front of the Al plate in a distance of $d = 7$ cm. A custom PCB connected the power and control signal to all individual drivers. It enabled bypassing the signals for individual slots, allowing more flexibility of the LED placement. The front was covered with a 3-mm-thick glass with high transparency in a wide spectral range, Schott B270 (Schott AG, Mainz, Germany). Another rubber gasket in a groove in the Al was used for sealing the front side as well and to protect the drivers and LEDs. Stainless steel plates were screwed into the Al plate, which extended over the glass and pressed it onto the groove. A small piece of rubber between the two prevented the steel from pressing directly onto the glass, which could cause glass breakage. Silicone paste was added for additional sealing on the outside edge between glass and Al. Drivers and connection PCB were, furthermore, sprayed with a plastic spray after assembly. These multiple sealing layers added redundancy to the protection of the electronics and LEDs. Furthermore, the sealing still allowed the front side to be opened for the purpose of changing components or the driver and LED layout. The basic design in SolidWorks (Dassault Systèmes, Vélizy-Villacoublay, France) is shown in Figure 5.

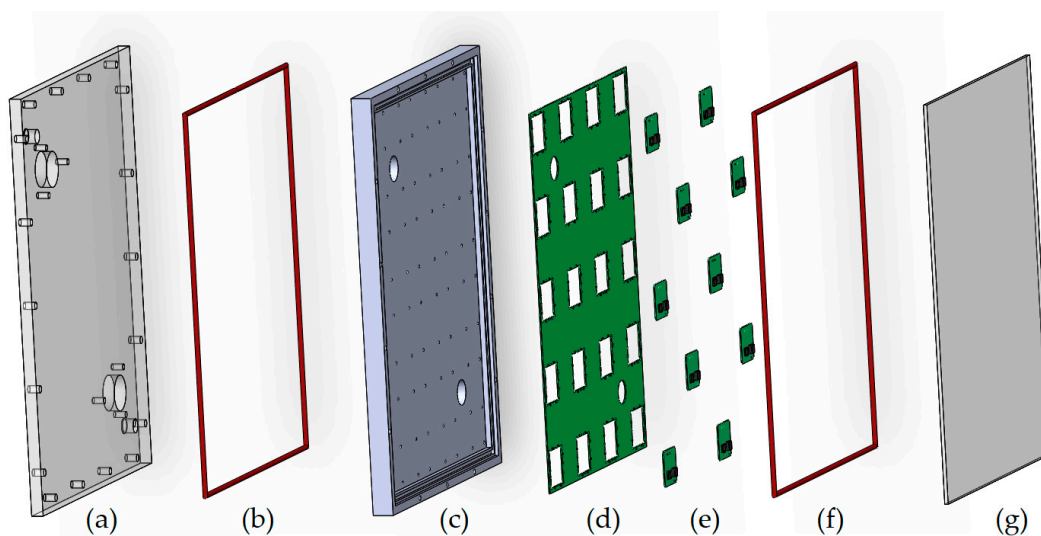


Figure 5. Designed layout of the array. (a) Plexiglas back cover. (b) Backside sealing. (c) Aluminum plate. (d) printed circuit board (PCB) for electrical connections. (e) Electronic drivers and LEDs. (f) Front side sealing. (g) Front glass cover.

Multiple plates can be connected in series or in parallel, including power and control signals as well as water cooling channels. This modular design enables an easy adjustment and possible upscaling of the array size to meet the specific requirements and target illuminated area.

3. Array Prototype Characterization

3.1. Array Manufacturing

We constructed a prototype of the array with one plate containing 10 commercially available LZ4-04UV00 LEDs (LED Engin Inc., San Jose, CA, USA), emitting light with a peak wavelength between 365 nm and 370 nm [32]. Pictures of the front and back of the array are shown in Figure 6. A generic water pump (unknown manufacturer, China) circulated water through plastic tubes to the array. An unbranded radiator and an EEC0382D2-000U-A99 fan (Sunonwealth Electric Machine Industry Co., Kaohsiung City, Taiwan) cooled the water. The fan and pump were operated with a 6205B Dual DC Power Supply (Hewlett Packard Enterprise, Palo Alto, CA, USA), enabling control of water and air flow and, thus, the cooling power of the systems.

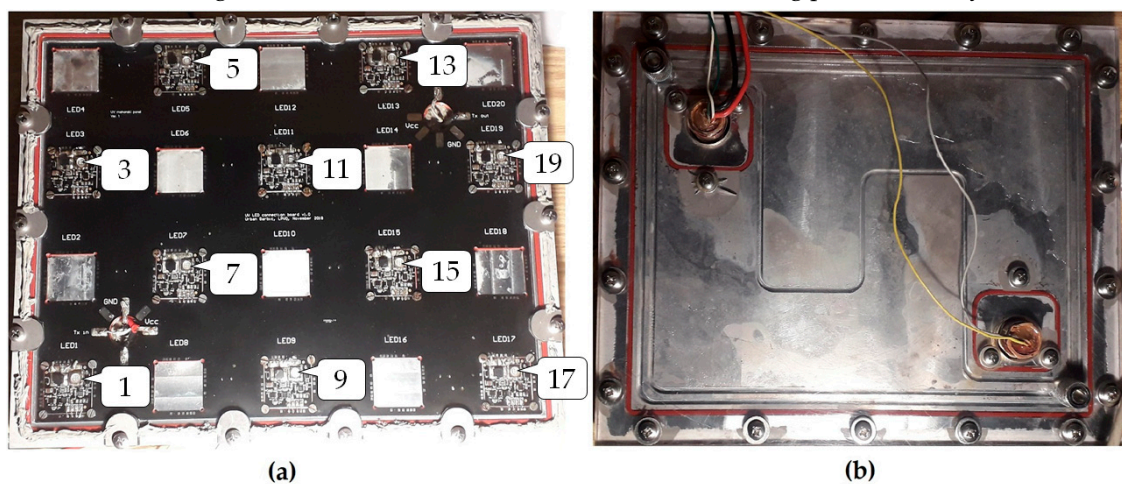


Figure 6. Prototype of the light source with 10 drivers and LEDs. (a) Light source front side, showing LED numbering and positioning used in this manuscript. (b) Light source back side.

3.2. Angular LED Radiance

Before optimizing the irradiance, we first tested the validity of the non-perfect Lambertian approximation by comparison with the measured angular irradiance of the LEDs. An integrating sphere and an S1336-8BQ photodiode (Hamamatsu Photonics K.K., Hamamatsu, Japan) were used to measure radiance around the LED between angles of $\theta = 90^\circ$ and -90° at a 3° step. After each sweep, the LED was rotated by $\phi = 15^\circ$. While the integrating sphere was not needed in these measurements, it did not change the measured relative irradiance at various angles. All together, 13 sets of measurements were taken, as shown in Figure 7.

The calculated distribution fit well with the measured one of the LZ4-04UV00 LEDs, with minor radiance differences at very high angles, as shown in Figure 8. This good fit depended strongly on the type of LED and the optical components used. The radiance profile of other LEDs might not be described as accurately with Equation (1).

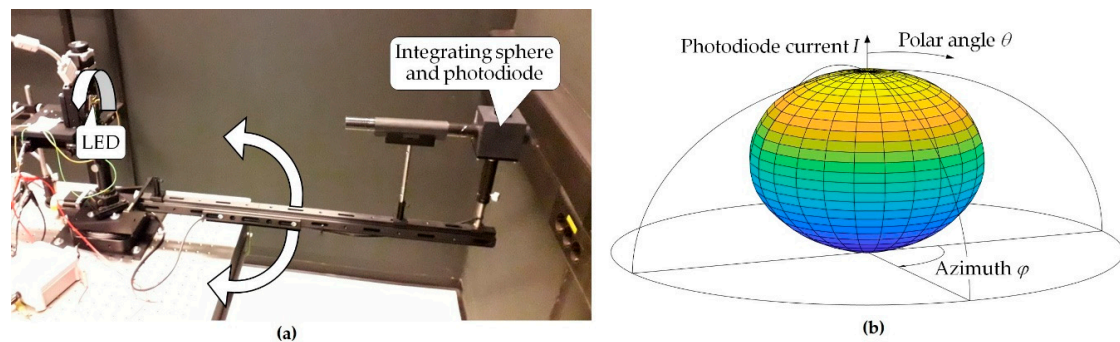


Figure 7. (a) Measurement setup for analyzing the angular distribution of LED radiance. (b) Measurements of an LED Engin LZ4-04UV00 in spherical coordinates, normalized to the peak value at $\theta = \phi = 0$. The azimuth ϕ describes LEDs' rotation. The θ is the polar angle between the position of the integrating sphere and the LEDs' main optical axis.

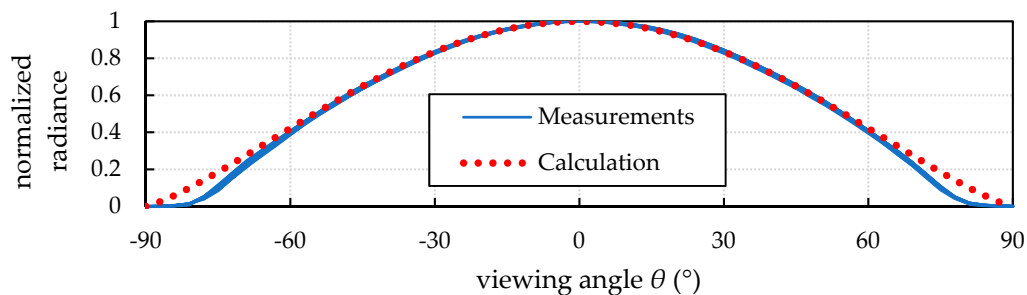


Figure 8. Comparison between 13 measurements of angular LED radiance and approximation with non-perfect Lambertian emitter.

3.3. Spatial Irradiance Profile

We optimized the irradiance with the method described in Section 2.1. Because of the small array size and inhomogeneous LED placement, some manual adjustments were needed for a better irradiance homogeneity. The distance between array and target object was set to 10 cm. LED placement is shown in Figure 6a. However, radiance variations of the different LEDs at the same operating current were expected, even within the same bin [32]. Thus, the radiance of the individual LEDs was measured at various currents with an integrating sphere and an S1336-8BQ photodiode for a relative comparison. The final settings for the array were then calculated using the radiance required from each LED and their individual current–radiance profile. We further measured the spectrum of the LEDs with an HR2000+ spectrometer and a CC-3-UV-S cosine corrector (both Ocean Optics Inc., Tampa, FL, USA) and compared them to find any possible outliers.

Then, the irradiance of the entire array was measured inside a black enclosure using an S1133-01 photodiode (Hamamatsu Photonics K.K., Hamamatsu, Japan) mounted on a stepper drive in a distance of 10 cm from the array. One scan every 2 mm was taken over an area of $15 \times 15 \text{ cm}^2$. The irradiance in (W/m^2) was then calculated from the area of the sensor as well as its spectral responsivity, obtained from the datasheet [33], and the measured LED spectrum. The array was operated at approximately 24% of its maximal radiance, i.e., the nominal power of the LEDs at the highest setting.

We then calculated the irradiance of the array with Equations (3) and (4). The optical LED power was set to 2.7 W, which was the center between minimal and maximal rated power of the LEDs within the corresponding bin according to the datasheet, -2.4 W and 3 W , respectively [32]. The required settings are given in Table 1. Measured and calculated irradiance were compared. We further used the optimization methods in MATLAB described in [21] to verify the results of the parameter optimization.

Table 1. Optimized values for the LED power and required settings. Due to variations in the individual radiance of the LEDs, some of them had to be operated at different currents to obtain the same output power. LEDs are numbered as they are in Figure 6a.

LED #	1	3	5	7	9	11	13	15	17	19
Rel. Power (%)	23.5	17.2	16.0	8.9	17.2	12.0	16.0	8.9	23.5	17.2
Setting (0-255)	57	36	40	28	46	25	34	19	60	44

3.4. Test in Climatic Chamber

Some applications require light sources to operate in extreme climatic conditions. To test the functionality of the array in such conditions, it was placed within a KK-2310 CHLT climatic chamber (Kambič d.o.o., Semič, Slovenia) after initial characterization. The temperature in the chamber was set to 80 °C and the array was operated at 50% of its maximal radiance. The water pump, radiator, and fan were placed outside the chamber. The temperature of the array was regulated by adjusting air and water flow. This temperature was measured by the microcontroller, which gave an indication of the temperature of the LEDs. However, some offset was expected, depending on the thermal resistance between the LED junction and package, package and driver, and driver and microcontroller. The other settings are given in Table 2.

Table 2. Climatic chamber settings and measured temperature by the microcontroller.

Relative Humidity (%)	20	50	80	50	20
Time (Days)	1	10	7	7	7
Array Temperature (°C)	50 ± 3	50 ± 3	60 ± 3	60 ± 3	60 ± 3

When the array was cooled down to (50 ± 3) °C, water was condensing on its surface at 50% relative humidity (RH). Thus, we reduced air and water flow to increase the temperature of the array to (60 ± 3) °C. At the highest set relative humidity (80%), some water was still condensing on the light source’s outer surface. However, no condensation was observed at the lower set RH values after this reduction.

This experiment was then extended to evaluate the resistance of the drivers and LEDs against the harsh conditions and possible failure of the light source’s components. The temperature was kept at 80 °C. Two additional cycles were carried out. In the first, the light source was operated at 25% maximum power, with RH in the chamber set to 10% (seven days) and 50% (seven days). In the second, the light source was operated at 10% maximum power, with the same RH settings and the same duration. The power of the individual LEDs was measured in between these steps with an integrating sphere and an S1336-8BQ photodiode (Hamamatsu Photonics K.K., Hamamatsu, Japan). After this experiment, the individual LED spectrum was measured again to analyze a possible spectral shift of the emitted light caused by the degradation.

4. Results

4.1. Driver Operation

The light source and all its components were working as expected. The driver had a very good linearity across the current range with both measured LEDs, enabling accurate control of individual LED radiance. The measured LED radiance at different driver settings is shown in Figure 9.

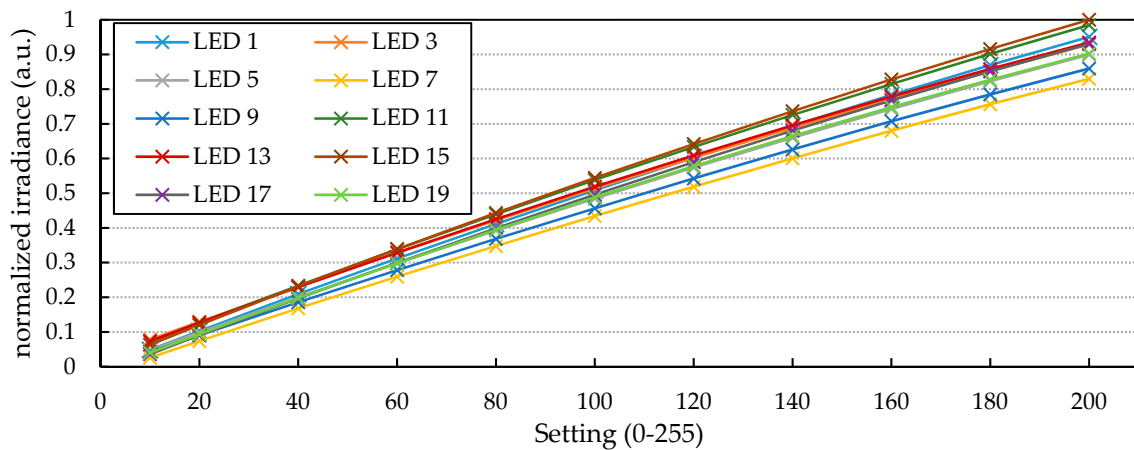


Figure 9. Radiance of 10 LEDs measured with a photodiode and an integrating sphere. The measured photodiode current is plotted against the digital setting of the LED current.

4.2. Irradiance Homogeneity

4.2.1. Optimization Method

Table 3 shows the comparison between our optimization method with manual adjustments and optimized reference values obtained with GA and PS algorithms. While there were differences of individual LED power, both methods led to a comparably good optimized irradiance homogeneity in the target area. The calculated standard deviations of the irradiance in the optimized $24 \times 18 \text{ cm}^2$ were 2.6% for the former and 3.4% for the latter. The non-uniformities were 13.8% and 14.1%, respectively. While the standard deviation was a measure of the general irradiance homogeneity, the non-uniformity was a measure of the spread between minimal measured irradiance E_{min} and maximal measured irradiance E_{max} . It is, for example, used for characterization of the spatial irradiance homogeneity of solar simulators [34]. It is defined as:

$$non - uniformity = \frac{E_{max} - E_{min}}{E_{max} + E_{min}} \times 100\%. \tag{6}$$

Table 3. Comparison between the iterative optimization method, described in Section 2.2, and, as reference, the Genetic Algorithm (GA) and Pattern Search (PS)-based methods in MATLAB. The values are normalized to their respective maximum.

LED #	1	3	5	7	9	11	13	15	17	19
Iterative (%)	100	73	68	38	73	51	68	38	100	73
GA/PS (%)	100	77	77	52	78	56	77	52	100	77

We further compared the irradiances in the optimized area before optimization, when all LEDs were set to 100%, and after optimization. The results are shown in Figure 10. The standard deviation beforehand was 7.3% and the non-uniformity was 21.6%. Optimizing the array resulted in a reduction of the standard deviation by a factor of 2.9 and a reduction of the non-uniformity by a factor of 1.6. However, this improvement came at the cost of a lower irradiance because it was gained by dimming LEDs.

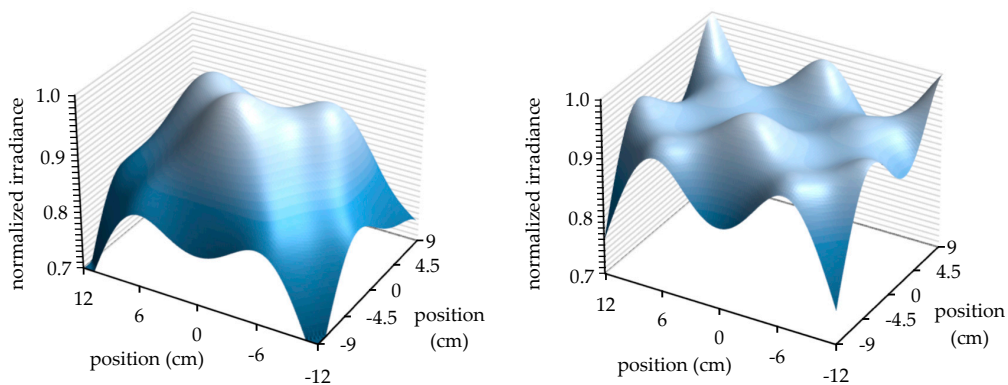


Figure 10. Calculated normalized irradiance before (left) and after (right) optimization.

4.2.2. Measurements

The irradiance measurement in the target plane, described in Section 3.3, is shown in Figure 11. The standard deviation was 1.8% over the analyzed area. The non-uniformity was 5.9%. This value was much smaller than the calculated one given before because of the limited measured area of $15 \times 15 \text{ cm}^2$.

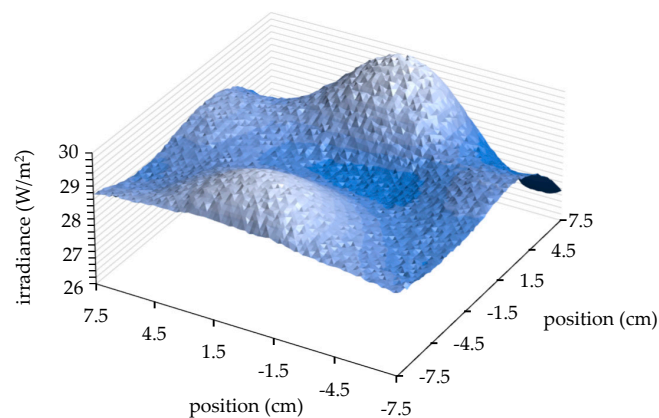


Figure 11. Measured irradiance in a $15 \times 15 \text{ cm}^2$ target area.

The comparison between measured and calculated irradiance yielded a good fit. The measured average irradiance was 28.6 W/m^2 and the calculated one was 25.2 W/m^2 . This calculation included a 10% loss due to the front glass transmissivity, previously measured by a Lambda 950 spectrometer (PerkinElmer, Waltham, MA, USA). Possible reasons for this underestimation are reflections inside the blackened enclosure, as well as an underestimation of the LED radiance according to the datasheet. Using the upper limit of the bin for the LED power, i.e., 3 W, the calculations yielded a radiance of 28.0 W/m^2 , which was well within the 10% tolerance the manufacturer keeps on the given irradiance values [32] of the measurement. Further deviations were expected due to differences of the angular radiance profile of the LEDs and its mathematical approximation. While the slight overestimation at high angles by assuming a non-perfect Lambertian angular radiance (Figure 8) had only minor influences on the irradiance profile, it led to an underestimation of I_{ij} calculated from the total LED radiance and, thus, to an underestimation of the calculated total irradiance.

Calculated and measured results were normalized to their respective average value for a comparison of the spatial irradiance profile. They yielded a good fit. The average pointwise difference between the two was 0.9% with the maximum of 3.2%, using one point for every measurement taken.

4.3. Characterization after Degradation

4.3.1. Total LED Radiance

The total LED radiance degrade over time, as can be seen in Figure 12. The average degradation was 7.5% during the first cycle and another 3.2% after the second cycle. It was strongest in LED 1 and LED 17, which were operated at the highest currents, and in LED 11. The corresponding driver of the latter failed during the second cycle. Some drivers failed during the third degradation cycle. Thus, no similar measurement was taken after it. Individual drivers had some issues already in the first two cycles, which were caused by weak soldering joints and were repaired.

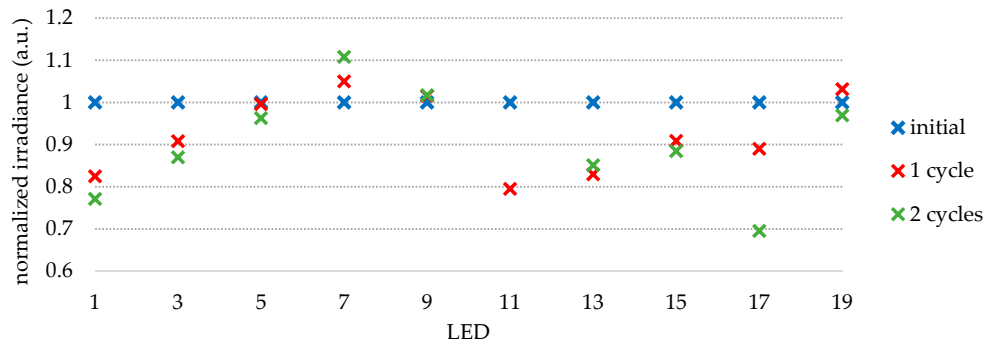


Figure 12. LED irradiance before and after the degradation cycles, normalized to their initial values. Degradation was strongest for the LEDs that were operated at the highest currents (1 and 17).

4.3.2. LED Radiance Spectrum

The spectral measurements of the LZ4-04UV00 LEDs are shown in Figure 13. The first set of measurements was taken after several initial tests with the light source, including one resulting in a failure of the sealing, shown in Section 3.4. While nine LEDs could be cleaned and salvaged after this incident, one had to be exchanged. The dashed blue line shows this new LED. The other LEDs already showed signs of early degradation, leading to a comparably higher half-width of the spectrum by emitting more light at higher wavelengths. The peak of all LEDs was at (367 ± 1) nm. The second set of measurements was taken after all three cycles of LED array degradation inside the climatic chamber. Because several drivers failed at this point, the LEDs were powered directly with an EA-PS 3032-10B power supply (EA Elektro-Automatik GmbH & Co. KG, Viersen, Germany). The half-width of the emission peak increased further. The peak wavelength shifted to (371 ± 2) nm. One outlier is shown by the dashed green line, LED 11. Visual inspection revealed a breakage of the cover lens of this LED and discoloration of the area beside the LED died, shown in Figure 14. The lenses cracked also on other LEDs. However, they exhibited no discoloration or stronger degradation.

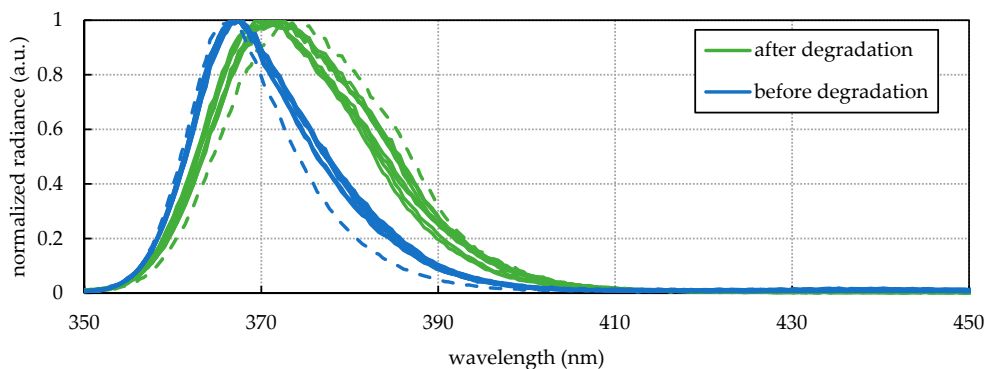


Figure 13. Spectral LED radiance, normalized to the maximum of each LED, before (blue) and after (green) climatic chamber tests. The dashed lines show outliers.

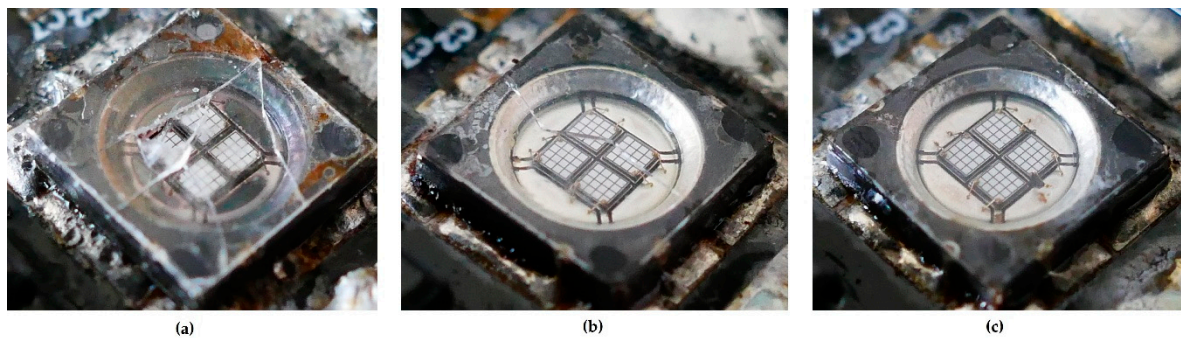


Figure 14. LEDs after degradation. (a) The front glass cover broke and the LED degraded severely. (b) The cover is cracked. However, it shows no other visible signs of degradation. (c) The cover is still intact and no degradation is visible.

4.4. Enclosure Sealing Failure

The multiple sealing layers for redundancy had not been added yet for the first test of the light source in the climatic chamber at 80 °C and 50% RH. Moist air was able to penetrate the sealing. It was condensing inside the sealed area due to the lower temperature of the water-cooled plate. Water accumulated in this area, causing severe corrosion of the drivers and failure of the array, shown in Figure 15. After this incident, additional layers of protection were added, as described in Section 2.3. The pressure of the front glass cover onto the rubber gasket was further increased. These results emphasized the importance of protecting LEDs and electronics sufficiently during use in similar environments.



Figure 15. Accumulated water inside the enclosure after around 63 hours in the chamber, caused by insufficient sealing.

5. Discussion

The advantage of the LED array presented in this paper is the modular design of all components. The drivers are able to set the current to the individual LEDs accurately, enabling full control over their radiance and, thus, the irradiance in the target area. The LED footprint on these modules allows mounting of various LEDs and corresponding spectral radiance currently on the market. The size of the drivers limits LED placement to approximately one LED every 3 cm × 3 cm. This modular design of both cooling system and LED drivers enables easy upscaling of the array to illuminate a larger target area.

Good agreement between measured and calculated irradiance was found using the approximation of LEDs as non-perfect Lambertian emitters. The only parameter required to describe their angular radiance profile is $\theta_{1/2}$, which is usually given in the datasheets. An underestimation of the calculations can be attributed to the LED's binning, spanning a large power range. Comparison between the spatial irradiance profiles normalized to the corresponding average found an only 0.9% average difference between the two. This good agreement enables prediction of the irradiance for larger arrays. For example, a $50 \times 50 \text{ cm}^2$ area can be irradiated with four similar plates containing 40 LEDs. The optimized irradiance, using the same LZ4-04UV00 LEDs, is 181.4 W/m^2 , with a standard deviation of 1.5% and non-homogeneity of 5.0%.

The LEDs showed moderate degradation at the elevated temperature and humidity in the chamber. The front cover of several LEDs cracked, which, in one case, was suspected to have caused additional damage due to the lack of protection. The LEDs driven at higher currents showed, in general, a higher degradation of the output power. Furthermore, the spectrum of the LEDs shifted after some time of use. The drivers degraded faster than the LEDs at elevated temperatures and humidity. After around two months inside the climatic chamber, multiple drivers failed and were not able to provide current to the LEDs anymore. The failed component could not be identified in all cases. Future work could enhance the stability of the light source in such environments for long-term use.

6. Conclusions

A modular, water-cooled LED array light source was developed and presented. LED radiance was controlled with novel custom electronic drivers. Modular layout of electronic drivers and cooling system as well as a general LED footprint enabled easy adjustment of the array for the required application. We calculated the irradiance and optimized its homogeneity on a flat target area for a prototype containing 10 LEDs. The results were compared with measurements, showing a good fit and a low standard deviation of the irradiance of 1.8%. The array and cooling system were tested at elevated temperature and relative humidity in a climatic chamber. While the cooling system was effective in reducing the array's temperature, LEDs and drivers still exhibited moderate degradation and a wavelength shift over time in the chamber.

Author Contributions: Conceptualization: All authors; methodology, S.M., Ž.R. and Ž.K.; software, S.M., Ž.R. and Ž.K.; validation, S.M., Ž.R. and Ž.K.; formal analysis, S.M. and Ž.R.; investigation, S.M. and Ž.K.; resources, M.T. and M.J.; data curation, S.M., Ž.R., Ž.K. and M.J.; writing—original draft preparation, S.M., Ž.R. and Ž.K.; writing—review and editing, all authors; visualization, S.M., Ž.R. and Ž.K.; supervision, M.T. and M.J.; project administration, M.T. and M.J.; funding acquisition, M.T. All authors have read and agreed to the published version of the manuscript.

Funding: This project received funding in part from the European Union's Horizon 2020 program in the framework of the project "SolarTrain" under Grant Agreement No. 721452 and in part from the Slovenian Research Agency (Javna agencija za raziskovalno dejavnost Republike Slovenije, ARRS) under the research program P2-0197.

Acknowledgments: The authors acknowledge the kind help of Matjaž Tome, Gašper Matič, and Matevž Bokalič, University of Ljubljana, for characterization and assembly of the array. Useful discussion with Matija Pirc, University of Ljubljana, for the design of the array is acknowledged. The PCB design for connecting the drivers by Urban Barbič, University of Ljubljana, is acknowledged. The LED footprint design by Matevž Bokalič, University of Ljubljana, is acknowledged.

Conflicts of Interest: The authors declare no conflict of interest. The funders had no role in the design of the study; in the collection, analyses, or interpretation of data; in the writing of the manuscript; or in the decision to publish the results.

References

1. Zissis, G.; Bertoldi, P. *Status of LED-Lighting World Market in 2017*; European Commission, JRC: Ispra, Italy, 2018; p. 1.
2. Dupuis, R.D.; Krames, M.R. History, development, and applications of high-brightness visible light-emitting diodes. *J. Lightwave Technol.* **2008**, *26*, 1154–1171. [[CrossRef](#)]

3. Muramoto, Y.; Kimura, M.; Nouda, S. Development and future of ultraviolet light-emitting diodes: UV-LED will replace the UV lamp. *Semicond. Sci. Technol.* **2014**, *29*, 084004. [[CrossRef](#)]
4. Schubert, E.F. *Light-Emitting Diodes*, 2nd ed.; Cambridge University Press: New York, NY, USA, 2006; pp. 201–236.
5. Kasap, S.O. *Optoelectronics and Photonics: Principles and Practices*; Prentice Hall: Upper Saddle River, NJ, USA, 2001; pp. 144–145.
6. Blankenbach, K.; Hertlein, F.; Hoffmann, S. Advances in automotive interior lighting concerning new LED approach and optical performance. *J. Soc. Inf. Disp.* **2020**, *28*, 655–667. [[CrossRef](#)]
7. Lin, K.-H.; Huang, M.-Y.; Huang, W.-D.; Hsu, M.-H.; Yang, Z.-W.; Yang, C.-M. The effects of red, blue, and white light-emitting diodes on the growth, development, and edible quality of hydroponically grown lettuce (*Lactuca sativa* L. var. capitata). *Sci. Hort.* **2013**, *150*, 86–91. [[CrossRef](#)]
8. Scherff, M.L.D.; Nutter, J.; Fuss-Kailuweit, P.; Suthues, J.; Brammer, T. Spectral mismatch and solar simulator quality factor in advanced LED solar simulators. *Jpn. J. Appl. Phys.* **2017**, *56*, 08MB24. [[CrossRef](#)]
9. Matafonova, G.; Batoev, V. Recent advances in application of UV light-emitting diodes for degrading organic pollutants in water through advanced oxidation processes: A review. *Water Res.* **2018**, *132*, 177–189. [[CrossRef](#)]
10. Hessling, M.; Gross, A.; Hoenes, K.; Rath, M.; Stangl, F.; Tritschler, H.; Sift, M. Efficient disinfection of tap and surface water with single high power 285 nm LED and square quartz tube. *Photonics* **2016**, *3*, 7. [[CrossRef](#)]
11. Davitt, K.; Song, Y.-K.; Patterson III, W.R.; Nurmikko, A.V.; Gherasimova, M.; Han, J.; Pan, Y.-L.; Chang, R.K. 290 and 340 nm UV LED arrays for fluorescence detection from single airborne particles. *Opt. Express* **2005**, *13*, 9548. [[CrossRef](#)]
12. Hubert, M.; Dimas, C.F.; Orava, P.; Koo, J. High-power UV LED array for curing photoadhesives. In Proceedings of the Applications of Photonic Technology, Quebec City, QC, Canada, 15 December 2003; pp. 163–168.
13. Hölz, K.; Lietard, J.; Somoza, M.M. High-power 365 nm UV LED mercury arc lamp replacement for photochemistry and chemical photolithography. *ACS Sustain. Chem. Eng.* **2017**, *5*, 828–834. [[CrossRef](#)]
14. Pirc, M.; Caserman, S.; Ferik, P.; Topič, M. Compact UV LED lamp with low heat emissions for biological research applications. *Electronics* **2019**, *8*, 343. [[CrossRef](#)]
15. Moreno, I.; Avendaño-Alejo, M.; Tzonchev, R.I. Designing light-emitting diode arrays for uniform near-field irradiance. *Appl. Opt.* **2006**, *45*, 2265. [[CrossRef](#)]
16. Rey-Barroso, L.; Burgos-Fernández, F.; Delpueyo, X.; Ares, M.; Royo, S.; Malveyh, J.; Puig, S.; Vilaseca, M. Visible and extended near-infrared multispectral imaging for skin cancer diagnosis. *Sensors* **2018**, *18*, 1441. [[CrossRef](#)] [[PubMed](#)]
17. Błaszczak, U.J.; Gryko, Ł.; Zając, A.S. Characterization of multi-emitter tuneable led source for endoscopic applications. *Metrol. Meas. Syst.* **2019**, *26*, 153–169. [[CrossRef](#)]
18. Bartczak, P.; Gebejes, A.; Falt, P.; Parkkinen, J.; Silfstein, P. Led-based spectrally tunable light source for camera characterization. In Proceedings of the 2015 Colour and Visual Computing Symposium (CVCS), Gjøvik, Norway, 25–26 August 2015; pp. 1–5.
19. Kagel, H.; Jacobs, H.; Bier, F.; Glöckler, J.; Frohme, M. A novel microtiter plate format high power open source LED array. *Photonics* **2019**, *6*, 17. [[CrossRef](#)]
20. Lei, P.; Wang, Q.; Zou, H. Designing LED array for uniform illumination based on local search algorithm. *J. Eur. Opt. Soc.-Rapid* **2014**, *9*. [[CrossRef](#)]
21. Rojec, Ž. Optical Optimization of LED Array in a Solar Simulator. Master's Thesis, University of Ljubljana, Ljubljana, Slovenia, 2014.
22. Kempe, M.D. Ultraviolet light test and evaluation methods for encapsulants of photovoltaic modules. *Sol. Energy Mater. Sol. Cells* **2010**, *94*, 246–253. [[CrossRef](#)]
23. Mansour, D.E.; Barretta, C.; Pitta Bauermann, L.; Oreski, G.; Schueler, A.; Philipp, D.; Gebhardt, P. Effect of Backsheet Properties on PV Encapsulant Degradation during Combined Accelerated Aging Tests. *Sustainability* **2020**, *12*, 5208. [[CrossRef](#)]
24. Jošt, M.; Albrecht, S.; Kegelmann, L.; Wolff, C.M.; Lang, F.; Lipovšek, B.; Krč, J.; Korte, L.; Neher, D.; Rech, B.; et al. Efficient light management by textured nanoimprinted layers for perovskite solar cells. *ACS Photonics* **2017**, *4*, 1232–1239. [[CrossRef](#)]

25. Owen-Bellini, M.; Hacke, P.; Miller, D.C.; Kempe, M.D.; Spataru, S.; Tanahashi, T.; Mitterhofer, S.; Jankovec, M.; Topič, M. Advancing reliability assessments of photovoltaic modules and materials using combined-accelerated stress testing. *Prog. Photovolt. Res. Appl.* **2020**, in press. [CrossRef]
26. Ndiaye, A.; Charki, A.; Kobi, A.; Kébé, C.M.; Ndiaye, P.A.; Sambou, V. Degradations of silicon photovoltaic modules: A literature review. *Sol. Energy* **2013**, *96*, 140–151. [CrossRef]
27. Cheng, H.H.; Huang, D.-S.; Lin, M.-T. Heat dissipation design and analysis of high power LED array using the finite element method. *Microelectron. Reliab.* **2012**, *52*, 905–911. [CrossRef]
28. Mitterhofer, S.; Jankovec, M.; Topič, M. A setup for in-situ measurements of potential and UV induced degradation of PV modules inside a climatic chamber. In Proceedings of the 53rd International Conference on Microelectronics, Devices and Materials MIDEM, Ljubljana, Slovenia, 4–6 October 2017; pp. 65–70.
29. Mitterhofer, S.; Jankovec, M.; Topic, M. Using UV LEDs for PV module aging and degradation study. In Proceedings of the 35th European Photovoltaic Solar Energy Conference and Exhibition, Brussels, Belgium, 24–28 September 2018; pp. 1323–1327. [CrossRef]
30. Wood, D. *Optoelectronic Semiconductor Devices*; Prentice Hall: New York, NY, USA, 1994; pp. 84–88.
31. Korošak, Ž. Modularno Svetilo iz Svetlečih Diod za Osvetljevanje Fotonapetostnih Modulov. Master's Thesis, University of Ljubljana, Ljubljana, Slovenia, 2018.
32. LED Engin LZ4-04UV00 Datasheet. Available online: <http://www.ledengin.com/files/products/LZ4/LZ4-04UV00.pdf> (accessed on 26 February 2020).
33. Hamamatsu Photonics S1087/S1133 Series Datasheet. Available online: https://www.hamamatsu.com/resources/pdf/ssd/s1087_etc_kspd1039e.pdf (accessed on 17 June 2020).
34. International Electrotechnical Commission. *IEC 60904-9:2020—Photovoltaic Devices—Part 9: Classification of Solar Simulator Characteristics*; International Electrotechnical Commission: Geneva, Switzerland, 2020; p. 10.

Publisher's Note: MDPI stays neutral with regard to jurisdictional claims in published maps and institutional affiliations.



© 2020 by the authors. Licensee MDPI, Basel, Switzerland. This article is an open access article distributed under the terms and conditions of the Creative Commons Attribution (CC BY) license (<http://creativecommons.org/licenses/by/4.0/>).